# Investigation of Hydroxyl Radical Yield in an Impact-Jet Hydraulic Cavitator


## *Authors:*

Yan Cao, Dongdong Xie, Yongchun Huang, Chengdu Huang, Kunming Zhang, Xiangyu Zhang, Shujun Wang



*Date Submitted:* 2023-02-20

*Keywords:* hydroxyl radical yield, hydrodynamic cavitation, prediction model, chitosan, degradation



*Abstract:*

Hydroxyl radical (·OH) is a key component that leads to the cleavage of the glycosidic bond in the process of chitosan (CS) degradation by hydrodynamic cavitation (HC). In this paper, methylene blue (MB) was selected as the trapping agent of ·OH and the yield of ·OH in an impact-jet hydraulic cavitator was investigated. The results showed that the cavitation intensity and the number of passes (N) were the two main factors affecting the yield of ·OH. A smaller cavitation number (Cv) or a larger N indicated that more ·OH can be produced. Based on the dimensionless number correlation method, the yield of ·OH was correlated with Cv, N, Euler number (Eu), Reynolds number (Re), and a dimensionless parameter (?), and a prediction model of ·OH yield was established. The relative deviations between the experimental and calculated values of the ·OH yield were basically within 10% by the prediction model. On the basis of the prediction model, the yield of ·OH produced in the process of CS degradation by HC was obtained. The results showed that the predicted yield of ·OH was significantly correlated with the intrinsic viscosity reduction rate of CS. It was suggested that the prediction model of ·OH yield based on the MB solution can be used to calculate the ·OH yield during the degradation of low concentration CS by HC.



*Record Type:* Published Article

*Submitted To:* LAPSE (Living Archive for Process Systems Engineering)

| | |
|---|---|
| *Citation (overall record, always the latest version):* | LAPSE:2023.0712 |
| *Citation (this specific file, latest version):* | LAPSE:2023.0712-1 |
| *Citation (this specific file, this version):* | LAPSE:2023.0712-1v1 |

*DOI of Published Version:* https://doi.org/10.3390/pr10112194

processes

MDPI

*Article*

# Investigation of Hydroxyl Radical Yield in an Impact-Jet Hydraulic Cavitator

**Yan Cao [1,2,*], Dongdong Xie [1], Yongchun Huang [1,2,*], Chengdu Huang [1,2], Kunming Zhang [1,2], Xiangyu Zhang [1] and Shujun Wang [3]**

[1] Department of Biological and Chemical Engineering, Guangxi University of Science and Technology, Liuzhou 545006, China
[2] Guangxi Key Laboratory of Green Processing of Sugar Resources, Guangxi University of Science and Technology, Liuzhou 545006, China
[3] National Key Laboratory of Food Nutrition and Safety, Tianjin University of Science and Technology, Tianjin 300457, China
* Correspondence: caoyan913@gxust.edu.cn (Y.C.); huangyc@yeah.net (Y.H.)

**Abstract:** Hydroxyl radical (·OH) is a key component that leads to the cleavage of the glycosidic bond in the process of chitosan (CS) degradation by hydrodynamic cavitation (HC). In this paper, methylene blue (MB) was selected as the trapping agent of ·OH and the yield of ·OH in an impact-jet hydraulic cavitator was investigated. The results showed that the cavitation intensity and the number of passes ($N$) were the two main factors affecting the yield of ·OH. A smaller cavitation number ($C_v$) or a larger $N$ indicated that more ·OH can be produced. Based on the dimensionless number correlation method, the yield of ·OH was correlated with $C_v$, $N$, Euler number ($Eu$), Reynolds number ($Re$), and a dimensionless parameter ($\gamma$), and a prediction model of ·OH yield was established. The relative deviations between the experimental and calculated values of the ·OH yield were basically within 10% by the prediction model. On the basis of the prediction model, the yield of ·OH produced in the process of CS degradation by HC was obtained. The results showed that the predicted yield of ·OH was significantly correlated with the intrinsic viscosity reduction rate of CS. It was suggested that the prediction model of ·OH yield based on the MB solution can be used to calculate the ·OH yield during the degradation of low concentration CS by HC.

**Keywords:** hydroxyl radical yield; hydrodynamic cavitation; prediction model; chitosan; degradation



**Citation:** Cao, Y.; Xie, D.; Huang, Y.; Huang, C.; Zhang, K.; Zhang, X.; Wang, S. Investigation of Hydroxyl Radical Yield in an Impact-Jet Hydraulic Cavitator. *Processes* **2022**, *10*, 2194. https://doi.org/10.3390/pr10112194

Academic Editor: Xiaodong Wu

Received: 10 October 2022
Accepted: 23 October 2022
Published: 26 October 2022



## 1. Introduction

Hydrodynamic cavitation (HC) is an emerging and green technology [1]. Since it has the advantages of simple operation, low cost, and low energy consumption, HC technology has been widely used in food processing [2], wastewater treatment [3], drug synthesis [4], emulsification [5], extraction [6], etc. In the process of HC, the collapse of cavitation bubble can produce instantaneous high temperature and high pressure, which can cause the splitting of water molecules trapped inside the bubble and the generation of hydroxyl radical (·OH) [7,8]. The ·OH has high activity and strong oxidation, which can intensify the chemical reaction process such as synthesis of chemicals, degradation of the water pollutants, etc. [9]

Low molecular weight chitosan (LMWC) [10,11] is the degradation product of high molecular weight chitosan (HMWC). Compared with the HMWC, LMWC has better solubility and superior functional properties such as anticancer activity [12], antifungal activity [13], enhancing immunity [14], disease resistance [15], etc. HC is a green technology that can be used to enhance the degradation of chitosan (CS) to obtain LMWC, which has attracted the attention of more and more scholars in recent years [16–19]. The degradation of CS is mainly caused by the mechanical effect and chemical effect (free radical effect) produced during the cavitation bubble collapse [20]. Yan et al. [21] pointed out that more

than 90% of the degradation of CS is caused by the chemical effect which is led to by the ·OH. The ·OH is the key component that led to the cleavage of the glycosidic bond. Therefore, the study of ·OH yield is of great significance for the regulation of CS degradation process.

·OH contains an unpaired electron in the outer valence orbitals which confers higher reactivity on it. ·OH is very unstable and its lifetime is very short (less than 1 μs) [22,23]. In order to evaluate the ·OH quantitatively, a trapping agent that can react with ·OH to form a stable product is usually used to remove ·OH [24–26] so that the amount of ·OH can be determined indirectly. Zupanca et al. [27] investigated the amount of ·OH formed in the process of HC by adding salicylic acid (an aromatic compound) as the trapping agent of ·OH to tap water. It was pointed out that the salicylic acid with low concentration was more suitable for the accurate determination of ·OH. Using KI as a trapping agent of ·OH, the effect of the HC flow generated by the orifice plate on the chemical reaction was studied by Kumar et al. [28] and Vichare et al. [29]. However, KI was sensitive to light and easy to decompose, which would lead to certain deviation in measurement. Zhang et al. [30] proposed a method of measuring the concentration of ·OH in cavitation flow by using methylene blue (MB) as trapping agent. The concentration of ·OH was obtained indirectly by measuring the absorbance of the MB solution. It was also pointed out that the collapse pressure of the cavity bubble was the exponential function of the measured concentration of ·OH. However, the above studies were all aimed at the generation of ·OH in the process of HC for the solutions with water as solvent. With regard to the complex system such as CS solution (CS dissolved in buffer solution) the quantitative experimental study of ·OH generated in the process of HC has not been reported. In the process of CS degradation by HC, ·OH will act on the glycosidic bond and be consumed rapidly [19], so it is difficult to directly determine the concentration of ·OH. In addition, it is also hard to quantitatively study the amount of ·OH by using trapping agent due to the competition between the ·OH trapping agent and degradation substances. Using the single-hole orifice plate as the cavitation generator, Zhang et al. [31] studied the effects of different factors on ·OH yield of a single cavitation bubble in the CS solution by the numerical simulation method. However, it is difficult to verify the results of this study by experiment.

The degradation of CS is closely related to the hydroxyl radical density. Therefore, the study on the yield of ·OH generated in the process of cavitation is helpful to further explore the degradation mechanism of CS. In order to make clear the relationship between the yield of ·OH and the degradation of CS in the process of HC, firstly, the influence of various factors on the yield of ·OH with the MB solution as the working medium was studied, and a prediction model for the yield of ·OH was established. Based on this model, the yield of ·OH formed in the process of CS degradation by HC was predicted, and the relationship between the predicted ·OH yield and the intrinsic viscosity reduction rate of CS was discussed. This study can provide a theoretical basis for the controllable degradation of CS and the optimized design of cavitation reactor.

## 2. Experimental Section

### 2.1. Materials

Methylene blue (AR grade) was provided by Tianjin Zhiyuan Chemical Reagent Co., Ltd., Tianjin, China. Chitosan with molecular weight of 1000 kDa and degree of deacetylation of 90% was obtained from Zhongfayuan Biological Technology Co., Ltd., Shenzheng, China. Acetic acid (AR grade) and sodium acetate trihydrate (AR grade) were purchased from Xilong Scientific Co., Ltd., Shantou, China. Pure water produced by a Milli-Q system (Millipore Co., Ltd., Billerica, MA, USA) was used to prepare various solutions.

### 2.2. Experimental Process Parameters

Two solutions were used in this study: the 16 μmol/L MB solution and the 0.3 g/L CS solution (CS dissolved in acetic acid/sodium acetate buffer solution with pH of 4.6). Each solution was preheated to the reaction temperature before carrying out the experiment. The parameters and conditions selected in the experiment were as follows: inlet pressure,

0.1–0.5 MPa; temperature, 30–70 °C; cavitation time, 10–90 min; throat diameter of cavitator, 0.5–0.9 mm; volume of solution, 120–240 mL.

### 2.3. Experimental Setup

Figure 1 shows the schematic diagram of the impact-jet HC setup used in this work. The solution (MB or CS) was delivered simultaneously by two gear pumps (WT3000-1JB, Longer Precision Pump Co., Ltd., Baoding, China). The pressure of the pipe was controlled by adjusting the speed of the gear pump. The pressure gauges (Y-40Z, Hongqi Instrument Co., Ltd., Leqing, China) were used to display the pressure values in real time. Two streams of fluid collided at the T-shaped junction and converged to form a stream of fluid, and then flowed into the venturi. ·OH was generated under the effect of cavitation. The fluid flowing from the end of the venturi returned to the beaker for cyclic cavitation. During the experiment, the temperature of the solution was controlled by a constant-temperature water bath (DF-101S, Gongyi Yuhua Instrument Co., Ltd., Zhengzhou, China). The size of water bath was determined by controlling the liquid level height of the water bath slightly higher than that of the solution in the beaker.

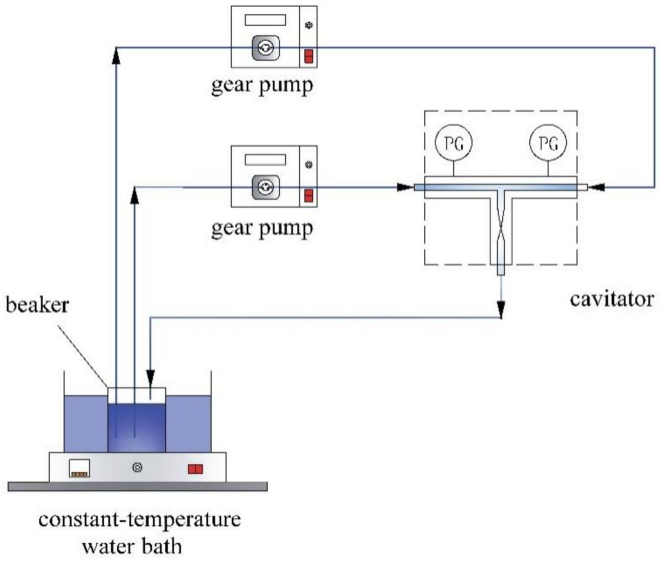


**Figure 1.** Schematic diagram of the impact-jet HC setup.

The schematic diagram of the impact-jet hydraulic cavitator is shown in Figure 2. The cavitator had two inlets and one outlet. The inner diameters of the inlet and outlet were 5 mm and 6 mm, respectively. The core component of the cavitator was the venturi with the throat diameter of 0.5–0.9 mm. The inlet cone angle and outlet cone angle of the venturi were 40° and 32°, respectively. The cavitator was made of polymethyl methacrylate (PMMA) with good transparency. The images of fluids flowing through the venturi were obtained by a camera (X-T20, Fuji Photo Film Co., Ltd., Tokyo, Japan), as shown in Figure 3. A micro-jet flow was observed at the end of the venturi throat. The micro-jet flow was a mechanical phenomenon caused by the pressure change, which can strengthen the contact of substances so that ·OH could be quickly captured.

### 2.4. Experimental Analysis

The absorbance of the MB solution before and after cavitation was measured by an ultraviolet-visible spectrometer (UV-2600, Shimadzu (china) Co., Ltd., Suzhou, China). The viscosity of the CS solution before and after cavitation was measured by a Ubbelohde viscometer. Density was measured by the density-bottle method. Surface tension was measured by a fully automatic interfacial tensiometer (JYW-2008, Chengde Kecheng Testing Machine Co., Ltd., Chengde, China).

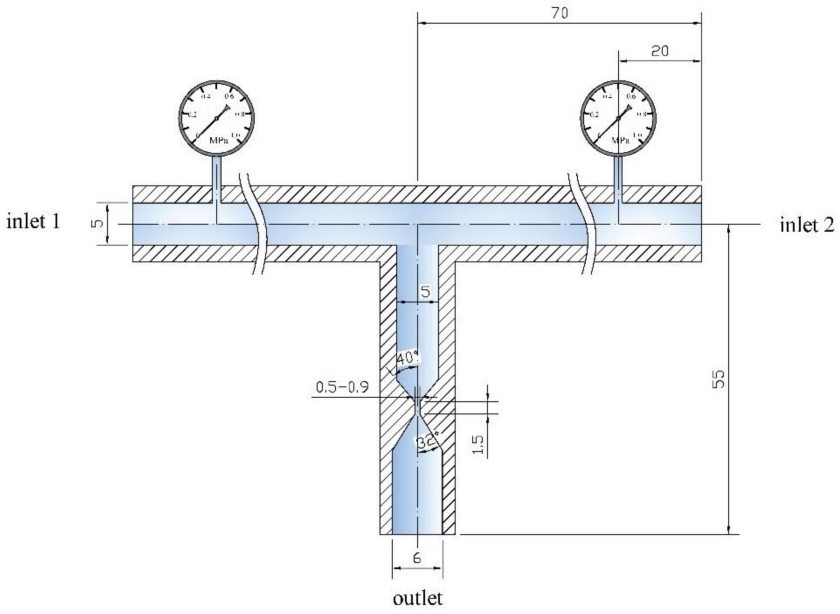


**Figure 2.** Schematic diagram of the impact-jet hydraulic cavitator. (The unit of length marked in the figure is mm.)

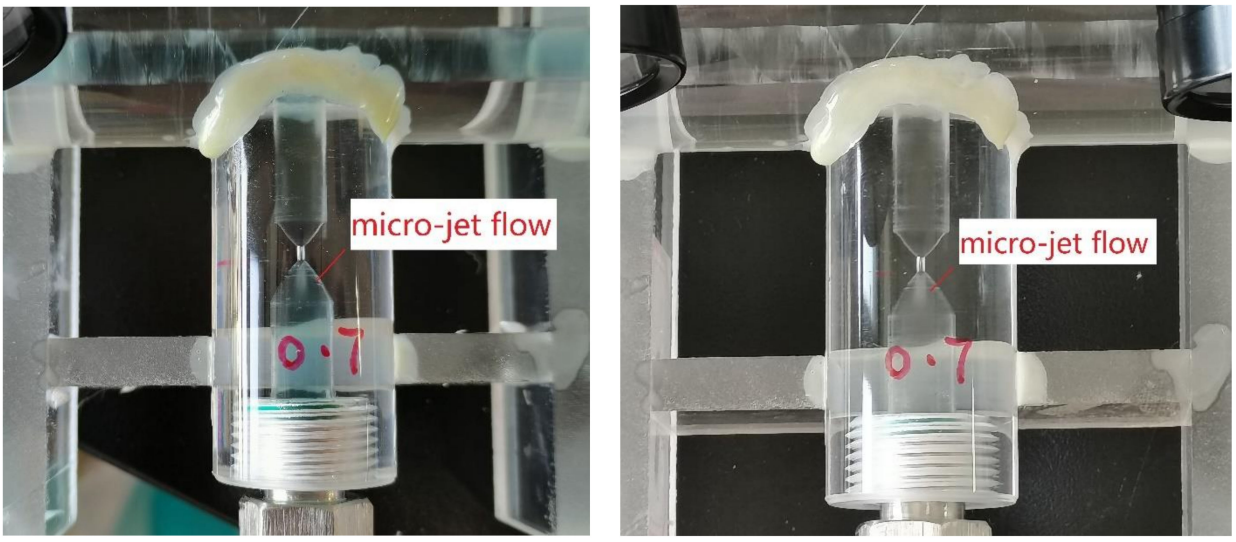


(**a**) MB solution (**b**) CS solution

**Figure 3.** Images of fluids flowing through the venturi (the images taken under the operation condition: throat diameter, 0.7 mm; inlet pressure, 0.4 MPa).

## 3. Results and Discussion

At low concentration, the absorbance of MB is linear with its concentration, which conforms to the Lambert–Beer law [32]. The standard curve of MB was established by measuring the absorbance of MB at different concentrations (4~20 μmol/L). Based on the fitted equation of the standard curve of MB, the concentration of MB can be calculated as follows:

$$C_{MB} = \frac{A - 0.0027}{0.033}, \quad (1)$$

where $A$ is the absorbance of MB.

MB reacts with ·OH to produce hydroxylated MB which is a stable oxidation product. The reaction formula is as follows:

$$\mathrm{MB} + \mathrm{OH} \rightarrow \mathrm{MB} - \mathrm{OH}. \tag{2}$$

The amount of ·OH produced by cavitation is the amount consumed by the reaction. Therefore, the amount of ·OH generated by cavitation can be calculated as follows:

$$C_{\cdot\mathrm{OH}} = C_{\mathrm{MB,o}} - C_{\mathrm{MB}} = \frac{A_{\mathrm{o}} - A}{0.033}, \tag{3}$$

where $C_{\mathrm{MB,o}}$ and $A_{\mathrm{o}}$ are the concentration and absorbance of MB before cavitation, respectively.

Cavitation number ($C_{\mathrm{v}}$) [33,34] is a dimensionless number which is mostly used to describe the characteristics of cavitating fluid. It can be defined as follows:

$$C_{\mathrm{v}} = \frac{P_{\mathrm{r}} - P_{\mathrm{v}}}{0.5\rho v^2}, \tag{4}$$

where $P_{\mathrm{r}}$ is the fully recovered downstream pressure, $P_{\mathrm{v}}$ is the saturated vapor pressure of the liquid at the operating temperature, $\rho$ is the density of the liquid, and $v$ is the average velocity of the liquid at the constriction. Under ideal conditions, cavitation occurs under the condition of $C_{\mathrm{v}} < 1$. The smaller the value of $C_{\mathrm{v}}$, the greater the cavitation intensity. Bagal et al. [35] have pointed out that the appropriate range of $C_{\mathrm{v}}$ was 0.1~1, within which the cavitation reactor can obtain the maximum benefits.

The cavitation effect is not only related to the intensity of cavitation, but also to the cavitation time. The influence of cavitation time on cavitation effect can be reflected by the number of passes of fluids through the hydraulic cavitator ($N$). $N$ is a dimensionless parameter, which can be described as follows [36]:

$$N = \frac{t}{t'} = \frac{Q}{V}t, \tag{5}$$

where $t$ is the cavitation time, $t'$ ($t' = V/Q$) is the residence time of the solution in the bath before next cycle, $Q$ and $V$ are the total flow rate and volume of the fluid, respectively.

### *3.1. ·OH Yield in MB Solution*

#### 3.1.1. Influence of Cavitation Time on ·OH Yield

Cavitation time is an important factor affecting the generation of ·OH. In this experiment, the influence of cavitation time on the yield of ·OH was studied, and the variations of $C_{\mathrm{v}}$ and $N$ values with cavitation time were discussed. The results are shown in Figure 4.

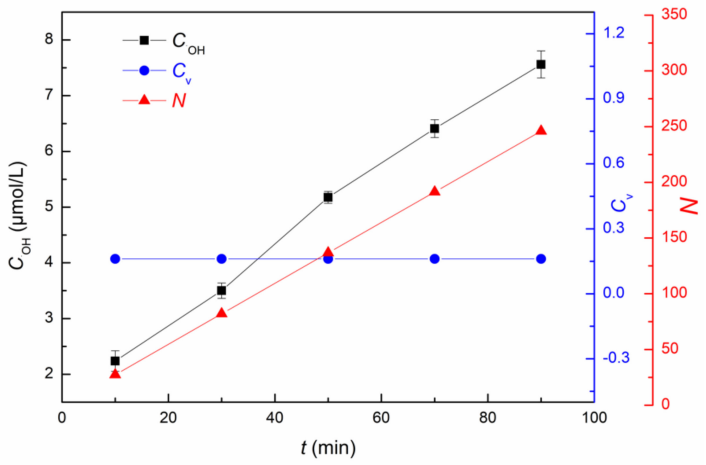


**Figure 4.** Influence of cavitation time on ·OH yield, $C_{\mathrm{v}}$ and $N$ values. (Conditions: $P_{\mathrm{i}}$ = 0.4 MPa, $T$ = 30 °C, $d$ = 0.5 mm, $V$ = 150 mL.)

As the cavitation time increased from 10 min to 90 min, the value of $C_v$ remained unchanged ($C_v$ = 0.161) while the yield of ·OH increased almost linearly. This was consistent with the experimental results of Amin et al. [37]. The value of $C_v$ remained unchanged, which indicated that the cavitation intensity did not change. However, $N$ increased from 27 to 246 with the increase in cavitation time. A larger $N$ indicated that the fluid was subject to cavitation more often, which led to an increase in the amount of cavitation bubbles produced in the liquid [38,39]. Zhang et al. [40] have pointed out that the amount of ·OH was proportional to the amount of cavitation bubble collapse. Therefore, under the condition that the cavitation intensity remained unchanged, the increase of $N$ contributed to the increase in ·OH yield.

#### 3.1.2. Influence of Throat Diameter on ·OH Yield

The constriction (throat of the venturi in this study) is the key part of the cavitation element, and its size can affect the amount of ·OH. Gogate and Pandit [41] have pointed out that the cavitation intensity decreased with the increase in the cross-sectional area at the constriction. The amount of ·OH depended on the cavitation intensity. The larger the cross-sectional area of the constriction, the less the amount of ·OH generated [37]. It was reported that a geometrical parameter ($\alpha$), which was the ratio of the constriction perimeter to the cross-sectional area of the constriction, can reflect the effect of the structure of constriction on cavitation intensity [1,4]. For the venturi used in this study, $\alpha$ can be calculated as follows:

$$\alpha = \frac{\pi d}{\frac{\pi}{4}d^2} = \frac{4}{d}, \quad (6)$$

where $d$ is the throat diameter. The larger the value of $a$, the greater the cavitation intensity.

In this experiment, the effects of throat diameter on ·OH yield, $C_v$, $N$, $v$, and $\alpha$ values were studied, as shown in Figure 5. With the increase in throat diameter from 0.5 mm to 0.9 mm, the amount of ·OH decreased from 5.369 μmol/L to 3.854 μmol/L, but the decrease in the amount of ·OH was not significant. At the same inlet pressure, the flow rate of the fluid increased with the increase in the throat diameter, and the average velocity ($v = 4Q/(\pi d^2)$) at the throat decreased, as shown in Figure 5. According to Equation (4), the value of $C_v$ increased with the decrease in the value of $v$, which indicated that the cavitation intensity was weakened. In addition, according to Equation (6), as the throat diameter increased, the value of $a$ decreased from 8000 to 4444, which also indicated that the cavitation intensity was weakened. Therefore, the amount of ·OH decreased with the increase in throat diameter. However, with the increase in throat diameter, the total flow rate of liquid increased. According to Equation (5), as the total flow rate of liquid increased, the value of $N$ increased from 137 to 377. The increase in the value of $N$ was conducive to the production of more ·OH, as discussed in Section 3.1.1. Both cavitation intensity and the number of passes affected the generation of ·OH. It was shown that the inhibition of ·OH production by the weakening of cavitation intensity was greater than the promotion of ·OH production by the increase in the number of passes. Therefore, the amount of ·OH decreased with the increase in throat diameter. The results of this work were consistent with those of Tao et al. [42].

#### 3.1.3. Influence of Inlet Pressure on ·OH Yield

HC is caused by the pressure change of the fluid flowing through the constriction of the cavitation equipment [5]. The pressure change is closely related to the free radical effect of cavitation. When the pressure in the recovery section remains unchanged, the inlet pressure becomes the main factor affecting the free radical effect of cavitation. Some studies have confirmed that better cavitation activity can be obtained at higher inlet pressure [43,44]. A similar conclusion was obtained in this study, as shown in Figure 6.

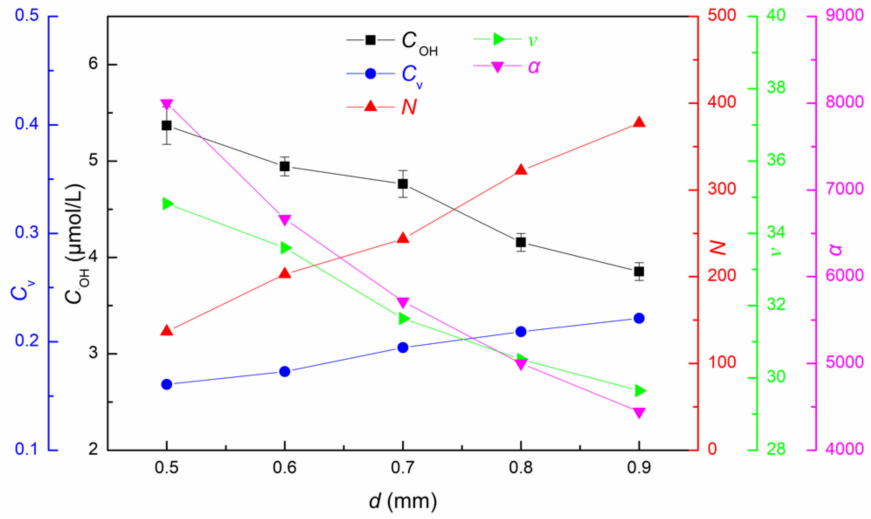


**Figure 5.** Influence of throat diameter on ·OH yield, $C_v$, $N$, $v$, and $\alpha$ values. (Conditions: $P_i$ = 0.4 MPa, $T$ = 30 °C, $t$ = 50 min, $V$ = 150 mL.).

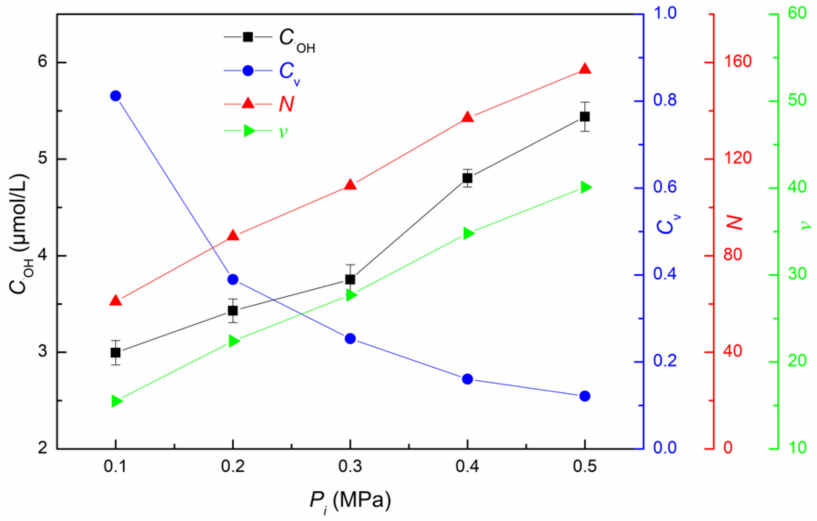


**Figure 6.** Influence of inlet pressure on ·OH yield, $C_v$, $N$, and $v$ values. (Conditions: $T$ = 30 °C, $d$ = 0.5 mm, $t$ = 50 min, $V$ = 150 mL).

With the increase in inlet pressure from 0.1 MPa to 0.5 MPa, the value of $C_v$ decreased from 0.812 to 0.121, and the yield of ·OH increased from 2.995 μmol/L to 5.439 μmol/L. When the inlet pressure increased, the pressure drop of the fluid through the constriction region increased, resulting in an increase in the collapse strength of a cavitation bubble [31]. Thus, more ·OH could be produced. It can be seen from Figure 6 that the average velocity of the fluid at the throat increased with the increase in the inlet pressure. The increase in the average velocity led to the decrease of $C_v$, indicating that the cavitation intensity increased. This was conducive to the production of ·OH. In addition, Figure 6 also illustrated that the value of $N$ increased with the increase in the inlet pressure. The increase in the number of passes was also conducive to the production of ·OH. Therefore, more hydroxyl radicals were produced at higher inlet pressure.

### 3.1.4. Influence of Solution Volume on ·OH Yield

According to Equation (5), the number of passes is related to the volume of the solution. Based on the discussion in the above sections, it has been known that the generation of ·OH was closely related to the number of passes, so it can be predicted that the volume of the solution can affect the yield of ·OH. In this experiment, the effects of solution volume

on ·OH yield, $C_v$, and $N$ values were investigated by changing the volume of solution from 120 mL to 240 mL. The results are shown in Figure 7.

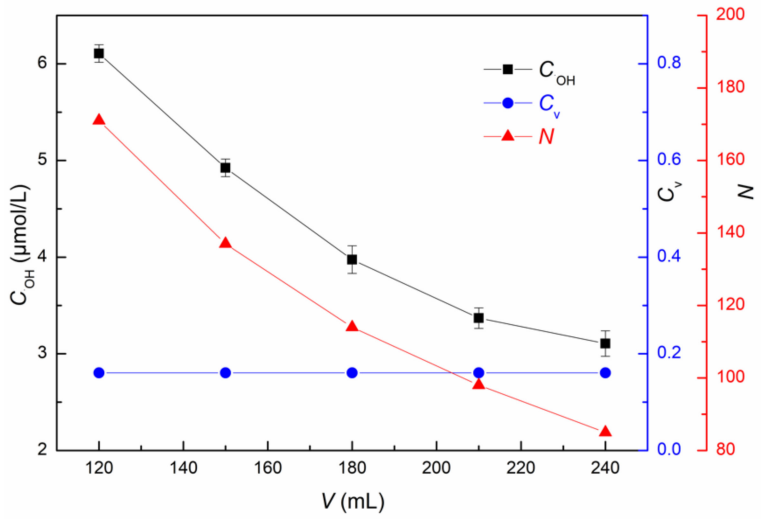


**Figure 7.** Influence of solution volume on ·OH yield, $C_v$, and $N$ values. (Conditions: $P_i$ = 0.4 MPa, $T$ = 30 °C, $d$ = 0.5 mm, $t$ = 50 min.)

When only changing the volume of the solution, the value of $C_v$ remained unchanged, which indicated that the cavitation intensity did not change. Thus, the number of passes became the main factor affecting the yield of ·OH. With the increase in the solution volume, the time required for the whole solution to complete one-time cavitation was increased. Thus, under a given cavitation time, the number of passes decreased from 171 to 85, as shown in Figure 7. A smaller value of $N$ indicated smaller amount of cavitation bubbles formed and collapsed in the process of HC, so that less ·OH was generated. Therefore, the yield of ·OH decreased with the increase in solution volume. It can be predicted that $N$ can be increased by prolonging the cavitation time, so as to achieve the high yield of ·OH for the large volume solution.

### 3.1.5. Influence of Temperature on ·OH Yield

The influence of temperature on the yield of ·OH, $C_v$, $N$, and $v$ values was studied, as shown in Figure 8. With the increase in temperature from 30 °C to 70 °C, the yield of ·OH increased from 4.606 μmol/L to 6.091 μmol/L. It was mainly attributed to the changes of the saturated vapor pressure and viscosity of liquid caused by the changes of temperature.

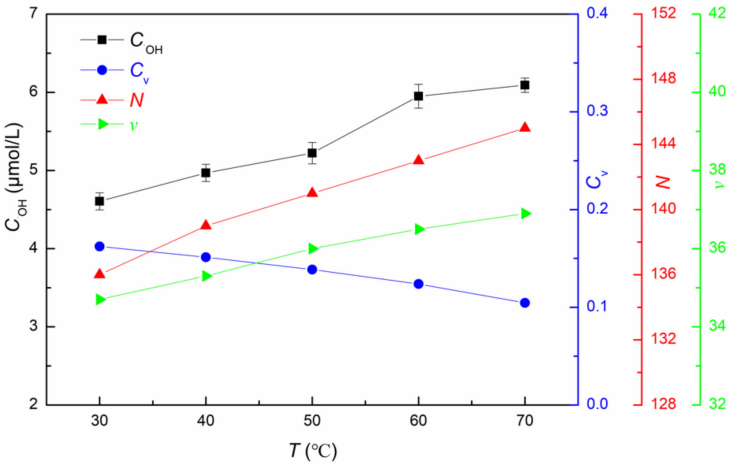


**Figure 8.** Influence of temperature on ·OH yield, $C_v$, $N$, and $v$ values. (Conditions: $P_i$ = 0.4 MPa, $d$ = 0.5 mm, $t$ = 50 min, $V$ = 150 mL.)

As the temperature increased, the saturated vapor pressure of liquid increased. Thus, the $C_v$ decreased and the cavitation effect increased. This was consistent with the conclusion that a higher vapor pressure indicated a higher chance of cavitation development [27]. In addition, with the increase in temperature, the viscosity of liquid decreased. At the same inlet pressure, the flow rate of liquid and the velocity at the throat increased. As can be seen from Figure 8, the velocity at the throat increased slightly, only from 34.7 m/s to 36.9 m/s. A small increase in the average velocity had a small impact on the $C_v$. Moreover, due to the small increase in flow rate of liquid, the value of $N$ only increased from 136 to 145. Although the increase in the average velocity of liquid and the number of passes was small, both of them were conducive to the production of ·OH. Furthermore, due to the decrease in liquid viscosity, the cavitation bubbles were easier to grow and collapse. Therefore, it was easier to promote the production of ·OH. Tao et al. [45] also proposed the similar conclusion that more ·OH can be generated at higher temperature.

#### 3.1.6. Prediction Model of ·OH Yield in MB Solution

Cavitation was considered to be the process of the formation, growth and rapid collapse of cavitation bubbles. The instantaneous high temperature and high pressure generated from the burst of the cavitation bubbles caused the dissociation of water molecules and the generation of ·OH. The generation of ·OH is not only related to the operating parameters, but also to the physical properties of the solution such as viscosity and surface tension [45]. Franc and Michel [46] pointed out that the change of physical characteristics of the solution can affect the behavior of a single cavitation bubble, so that the generation of ·OH can be affected. It was reported that the viscosity and surface tension of the solution had an impact on the cavitation process, such as supercavity detachment and cavitation inception [27], and the degree of influence increased with the decrease in spatial scale [47]. Viscosity tended to slow down the explosion and collapse of cavitation bubbles, especially for high viscosity liquids. Surface tension can accelerate the collapse of cavitation bubbles and affect the stability of cavitation bubbles. Therefore, the effects of viscosity and surface tension on the generation of ·OH cannot be ignored.

Zhang et al. [30] proposed a correlation equation between the concentration of ·OH measured experimentally and the collapse pressures predicted theoretically, which showed that the collapse pressure was exponentially related to the concentration of ·OH. Tao et al. [45] have proposed that in order to realize the controllability of cavitation process, a generalized correlation between ·OH generation and operating parameters and characteristic time scale should be developed. However, yield of ·OH was not only related to the operating parameters, but also to the physical and structural parameters.

Operating parameters and physical parameters can be reflected by some dimensionless numbers. Euler number ($Eu = \triangle p/(\rho v^2)$) is a dimensionless number which reflects the relative relationship between the pressure drop in the flow field and its dynamic head. It is well known that Reynolds number ($Re = dv\rho/\mu$) is the ratio of inertial force to viscous force which represents the effect of viscosity. Weber number ($We = \rho v^2 d/\sigma$) is a dimensionless number which represents the ratio of inertial force to surface tension force. It can be considered that the $C_v$, $N$, and $Eu$ are the dimensionless numbers that can reflect the effects of operating conditions on the generation of ·OH, and the $Re$ and $We$ are the dimensionless numbers that can reflect the effects of physical conditions on the generation of ·OH. In addition, a dimensionless parameter ($\gamma$) which can reflect the effects of structure conditions on the generation of ·OH was introduced in this study. It can be defined as follows:

$$\gamma = \frac{d}{D}, \tag{7}$$

where $D$ is the inner diameter of the pipe.

It has been reported that the model can be constructed by dimensionless number correlation method. Li et al. [48] and Cao et al. [49] have established the correlation equations between the correction factor of mass transfer coefficient and the different dimensionless

numbers based on the dimensionless number correlation method. Su et al. [50] proposed the correlation equation between the overall mean mass transfer coefficient (*ka*) and *Re*. Similarly, in order to comprehensively reflect the influence of various factors on the production of ·OH, the yield of ·OH was correlated with the above three types of dimensionless numbers based on the dimensionless number correlation method. A generalized correlation equation of ·OH yield was obtained, as shown in Equation (8).

$$C_{\cdot OH} = n_1 + n_2(n_3 C_V{}^a N^b + n_4 Eu^c + n_5 Re^d We^e)\gamma^f, \quad (8)$$

where $C_vN$ and *ReWe* as the combinations of dimensionless numbers reflected the influence of operating parameters and physical parameters on the ·OH yield, respectively.

The fitting result for Equation (8) was obtained by the optimization method of Levenberg–Marquardt and Universal Global Optimization in the software of 1stOpt (Version 1.5, 7D-Soft High Technology Inc., Beijing, China, 2006), as shown in Equation (9):

$$C_{\cdot OH} = 3.339 + 0.0007 \times (0.0027 C_V{}^{0.046} N^{1.06} - 0.786 Eu^{0.981} + 9.331 \times 10^{-12} Re^{6.227} We^{-4.559})\gamma^{-4.032} \quad (9)$$

The value of the correlation coefficient $R^2$ was 0.963.

The experimental and calculated values of the ·OH yield were compared and the result is shown in Figure 9. The relative deviations between the experimental and calculated values were within 10%. Therefore, it was reasonable to carry out theoretical calculation for ·OH yield by the theoretical model. This model can be used not only to predict the yield of ·OH in the MB solution, but also the yield of ·OH in other systems with the physical conditions similar to the MB solution.

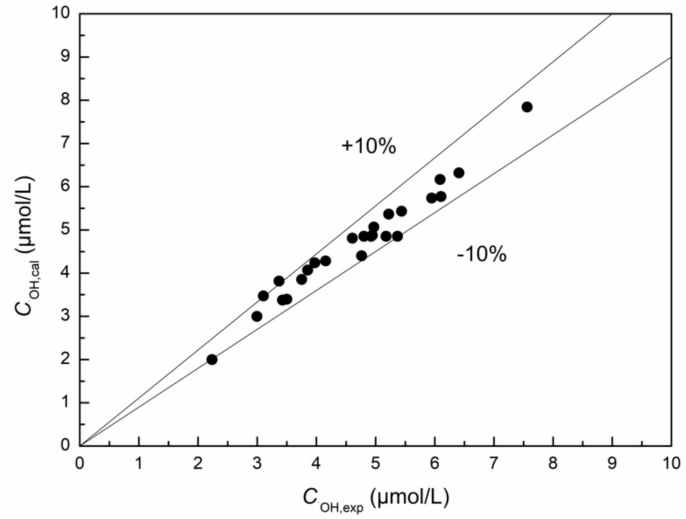


**Figure 9.** Comparison of experimental and calculated values for ·OH yield.

### *3.2. ·OH Yield in CS Solution*

The degradation process of CS by HC is the process of the cleavage of the glycosidic bond, in which the long-chain CS is transformed into the short-chain CS. In the process of CS degradation, both mechanical shear effect and free radical chemical effect can cause the breaking of glycosidic bond, but the latter contributes much more than the former [21]. Figure 10 shows the formation of ·OH and the degradation process of CS under the action of ·OH.

The viscosity of CS decreased with the degradation process. The degradation degree of CS can be reflected by the intrinsic viscosity reduction rate ($\eta$) [19] which can be defined as follows:

$$\eta = \frac{[\eta]_0 - [\eta]_1}{[\eta]_0} \times 100\%, \quad (10)$$

where $[\eta]_0$ is the intrinsic viscosity of the initial CS solution, and $[\eta]_1$ is the intrinsic viscosity of the CS solution after degradation. The intrinsic viscosity ($[\eta]$) is defined as follows:

$$[\eta] = \frac{\eta_{sp} + 3\ln\eta_r}{4c}, \tag{11}$$

where $\eta_{sp}$ is the specific viscosity ($\eta_{sp} = \eta_r - 1$), $c$ is the concentration of the CS solution, and $\eta_r$ is the relative viscosity ($\eta_r = t_s/t_p$) in which $t_s$ and $t_p$ are the efflux time of the CS solution and acetic acid/sodium acetate buffer solution measured by the Ubbelohde viscometer, respectively.

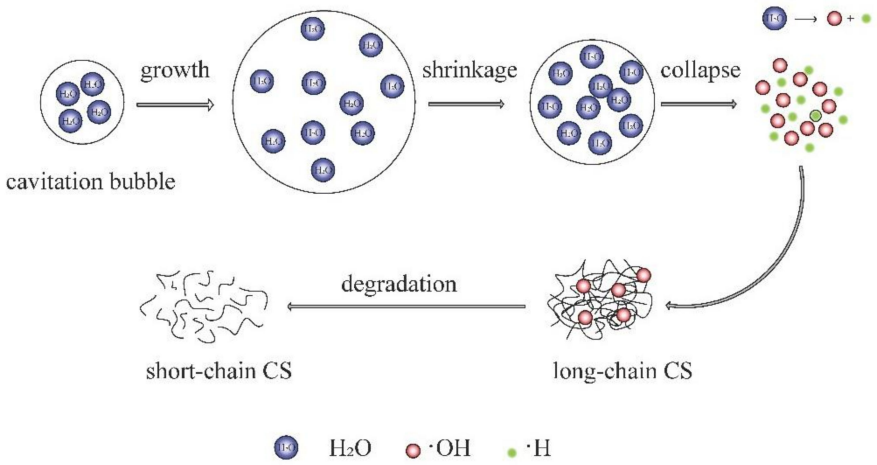


**Figure 10.** The processes of the formation of ·OH and the degradation of CS.

3.2.1. Influence of Various Factors on the Intrinsic Viscosity Reduction Rate of CS

As the working system, the 0.3 g/L CS solution was chosen. Under the same experimental conditions as the study of ·OH yield in the MB solution, the effects of various factors on the intrinsic viscosity reduction rate of CS were investigated. The results are shown in Figure 11.

Figure 11a–e was compared with Figures 4–8. It was found that the change trend of $C_v$ in the CS solution and in the MB solution was similar, and the change trend of the intrinsic viscosity reduction rate of CS was similar to that of the ·OH yield in the MB solution. It can be explained that the generation mechanism of ·OH in the MB solution and the CS solution was the same, both of which were generated by the dissociation of water molecules trapped inside the bubbles [27]. Therefore, the influence of various factors on $C_v$ was similar in these two dilute solutions. Furthermore, the degradation of CS was mainly caused by the free radical effect of cavitation. The ·OH generated in the process of HC can act on the β-1, 4 glycosidic bond of CS and cause the breaking down of CS chain [14,51]. A smaller value of $C_v$ indicated that more ·OH were produced, and more glycosidic bonds were broken down. Thus, the higher the yield of ·OH, the greater the intrinsic viscosity reduction rate of CS. The yield of ·OH was crucial to the degradation of CS. Therefore, it was of great significance to make clear the yield of ·OH in the process of CS degradation by HC, which was helpful in exploring the mechanism of CS degradation.

3.2.2. Prediction of ·OH Yield in CS Solution

It was reported that ·OH was a significant free radical for the degradation of CS [52]. The production of ·OH was closely related to the operation, physical and structural parameters. Therefore, the physical properties (density, viscosity, and surface tension) of the 0.3 g/L CS solution and the 16 μmol/L MB solution at different temperatures were measured in this work (as shown in Table 1).

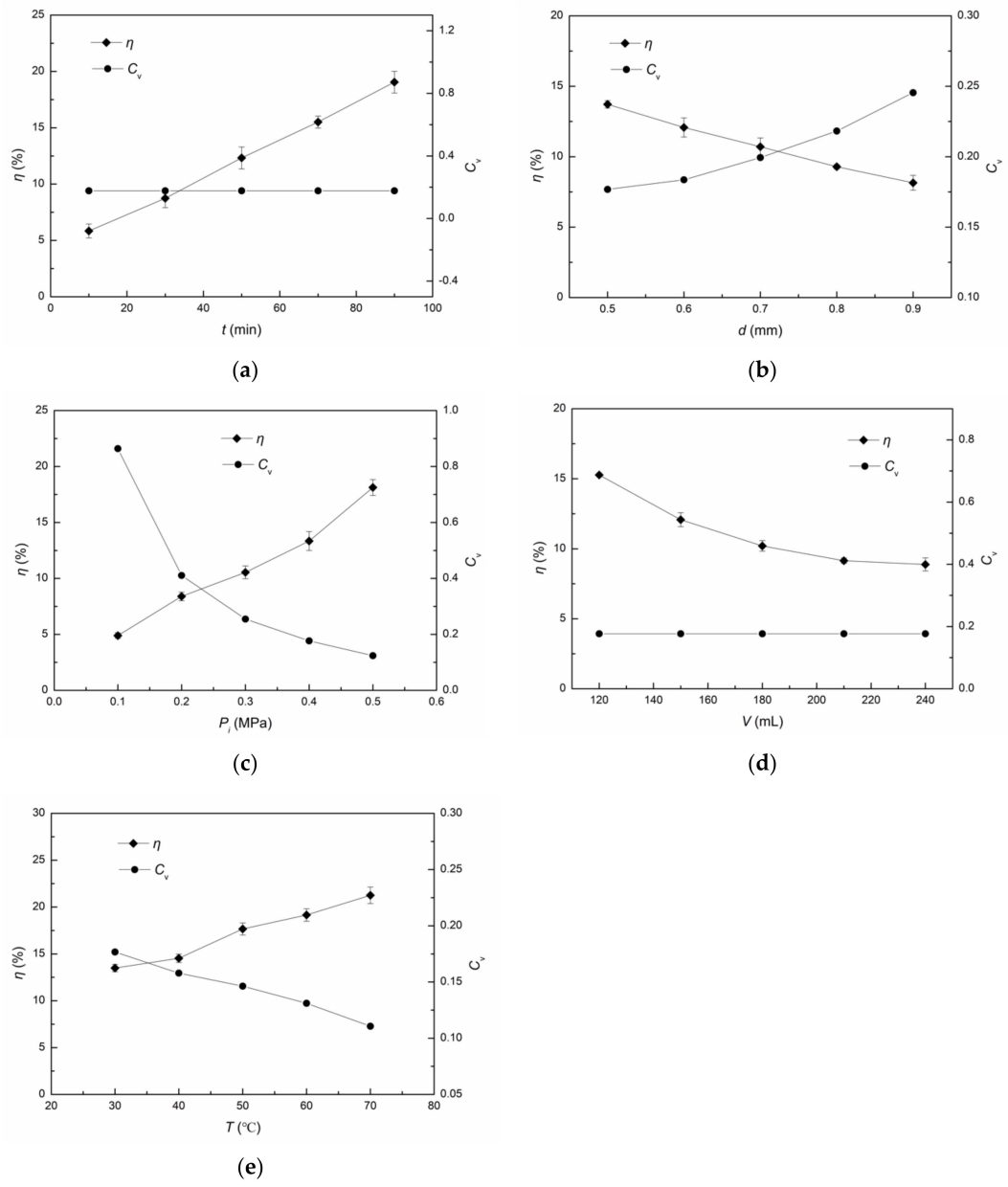


**Figure 11.** Influence of various factors on the intrinsic viscosity reduction rate of CS. Influence factors: (**a**) cavitation time; (**b**) throat diameter; (**c**) inlet pressure; (**d**) solution volume; (**e**) temperature.

**Table 1.** Physical properties of MB solution and CS solution at different temperatures.

| Solution | Temperature (°C) | Density (kg/m$^3$) | Viscosity (mPa·s) | Surface Tension (mN/m) |
|---|---|---|---|---|
| MB solution | 30 | 996.3 | 0.81 | 66.30 |
| | 40 | 994.5 | 0.66 | 64.93 |
| | 50 | 989.5 | 0.56 | 61.49 |
| | 60 | 987.4 | 0.48 | 57.88 |
| | 70 | 983.4 | 0.44 | 57.24 |
| CS solution | 30 | 1000.6 | 1.07 | 68.83 |
| | 40 | 998.4 | 0.89 | 67.77 |
| | 50 | 995.7 | 0.73 | 67.30 |
| | 60 | 991.2 | 0.61 | 66.57 |
| | 70 | 987.1 | 0.52 | 65.59 |

It can be seen from Table 1 that the density, viscosity and surface tension of the CS solution were larger than those of the MB solution, but the difference was not significant. In Section 3.1.6, a prediction model (Equation (9)) of ·OH yield was established based on the MB solution. This model was applied to the CS solution which had little difference in physical properties compared with the MB solution, and the yield of ·OH produced during the degradation of CS by HC was predicted. The relationship between the measured ·OH yield in the MB solution, the ·OH yield in the CS solution calculated using the prediction model, and the intrinsic viscosity reduction rate of CS was shown in Figure 12, in which 25 experimental points were taken as the abscissa.

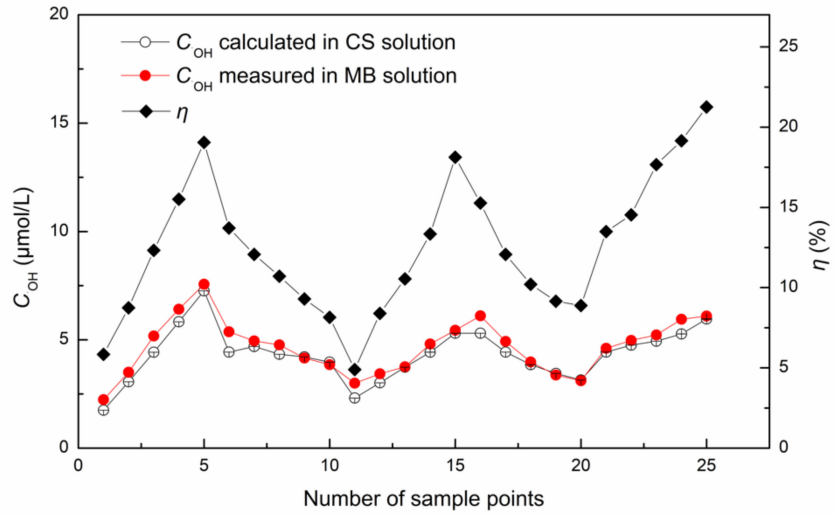


**Figure 12.** Comparison of measured ·OH yield in MB solution, calculated ·OH yield in CS solution, and intrinsic viscosity reduction rate of CS. Experimental points: 1–5 for cavitation time, 10–90 min; 6–10 for throat diameter, 0.5–0.9 mm; 11–15 for inlet pressure, 0.1–0.5 MPa; 16–20 for solution volume, 120–240 mL; 21–25 for temperature, 30–70 °C.

In general, the ·OH yield predicted in the CS solution was slightly lower than that measured in the MB solution. This was because under the same operating and structural conditions, the amount of ·OH was mainly affected by the physical properties of the solution, while there were some differences in physical properties between the CS solution and the MB solution. In comparison with the MB solution, the CS solution had higher viscosity, so it had smaller flow rate under the same pressure. In consequence, the value of $N$ was smaller and the value of $C_v$ was larger for the CS solution, which indicated that the cavitation effect generated in the CS solution was weaker than that in the MB solution under the same conditions. Based on the discussion in Section 3.1.6, it was found that the surface tension can accelerate the collapse of cavitation bubbles and lead to a higher collapse temperature and pressure. The inhibition of higher viscosity of the CS solution on the production of ·OH was slightly higher than the promotion of higher surface tension on the production of ·OH. Thus, the predicted yield of ·OH in the CS solution was slightly lower than that measured in the MB solution.

The change trend of ·OH yield predicted in the CS solution was consistent with that of the intrinsic viscosity reduction rate of CS, which further verified that the free radical effect was the main effect of CS degradation by HC [21]. Based on the software of IBM SPSS Statistics (Version 25, IBM Corp., New York, NY, USA, 2017), the correlation between the ·OH yield predicted in the CS solution and the intrinsic viscosity reduction rate of CS at 25 experimental points was analyzed. The result showed that the correlation (Pearson) was significant at the 0.01 level (2-tailed), which indicated that there was an obvious correlation between the ·OH yield predicted in the CS solution and the intrinsic viscosity reduction rate of CS. Therefore, it was reasonable to use the prediction model (Equation (9)) to predict the yield of ·OH generated in the low concentration CS solution.

## 4. Conclusions

The yield of ·OH in the MB solution was investigated in an impact-jet hydraulic cavitator. The effects of various parameters including cavitation time, throat diameter, inlet pressure, solution volume, and temperature on the yield of ·OH were studied. It was found that the yield of ·OH was affected by the operation, structure and physical parameters of solution, and the cavitation intensity and the number of passes were the two main factors affecting the yield of ·OH. A smaller cavitation number ($C_v$) or a larger $N$ indicated that more ·OH could be produced. Based on the dimensionless number correlation method, the yield of ·OH was correlated with $C_v$, $N$, $Eu$, $Re$, and $\gamma$. A prediction model of ·OH yield was established as follows:

$$C_{\cdot OH} = 3.339 + 0.0007 \times (0.0027{C_V}^{0.046}N^{1.06} - 0.786Eu^{0.981} + 9.331 \times 10^{-12}Re^{6.227}We^{-4.559})\gamma^{-4.032}.$$

The value of the correlation coefficient $R^2$ is 0.963. The relative deviations between the experimental and calculated values of the ·OH yield were basically within 10% by the prediction model. Furthermore, the effects of various parameters on the intrinsic viscosity reduction rate of CS were discussed. On the basis of the experimental data, the yield of ·OH produced in the process of CS degradation by HC was obtained by the established prediction model. The correlation between the predicted ·OH yield in the CS solution and the intrinsic viscosity reduction rate of CS was analyzed by IBM SPSS Statistics. The correlation (Pearson) was significant at the 0.01 level (2-tailed), which indicated that the predicted yield of ·OH was significantly correlated with the intrinsic viscosity reduction rate of CS. It was suggested that the prediction model of ·OH yield based on the MB solution can be used to calculate the ·OH yield during the degradation of low concentration CS by HC. This paper provides a new way for the study of ·OH yield in the CS solution, which will help to further study the degradation mechanism of CS and the optimized design of cavitation reactor.

**Author Contributions:** Conceptualization, Y.C. and K.Z.; methodology, Y.C. and S.W.; software, X.Z. and C.H.; validation, S.W.; investigation, D.X. and X.Z.; resources, K.Z.; data curation, D.X. and C.H; writing—original draft preparation, Y.C.; writing—review and editing, Y.H. and S.W.; visualization, K.Z.; project administration, Y.H.; funding acquisition, Y.H. and Y.C. All authors have read and agreed to the published version of the manuscript.

**Funding:** This research was funded by the National Natural Science Foundation of China, grant no. 31660472 and the Specific Research Project of Guangxi for Research Bases and Talents, grant no. Guike AD20238033.

**Data Availability Statement:** The data that support the findings of this study are available from the corresponding authors upon reasonable request.

**Acknowledgments:** The authors gratefully acknowledge the financial support of the National Natural Science Foundation of China (No. 31660472) and the Specific Research Project of Guangxi for Research Bases and Talents (No. Guike AD20238033).

**Conflicts of Interest:** The authors declare that they have no known competing financial interest or personal relationships that could have appeared to influence the work reported in this paper.

## Nomenclature

| | |
|---|---|
| $A$ | absorbance |
| $c$ | concentration of CS solution, g/L |
| $C_{MB}$ | concentration of MB solution, μmol/L |
| $C_{\cdot OH}$ | concentration of ·OH, μmol/L |
| $C_v$ | Cavitation number |
| $d$ | throat diameter, m |
| $D$ | inner diameter of pipe, m |
| $Eu$ | Euler number |
| $n_{1–5}$ | correction factor |

| | |
|---|---|
| $N$ | number of passes |
| $p$ | pressure, MPa |
| $P_r$ | fully recovered downstream pressure, MPa |
| $P_v$ | saturated vapor pressure, · |
| $Q$ | total flow rate of fluid, $m^3/s$ |
| $Re$ | Reynolds number |
| $t$ | cavitation time, s |
| $t'$ | residence time of the solution in the bath before next cycle, s |
| $t_p$ | efflux time of acetic acid/sodium acetate buffer solution measured by the Ubbelohde viscometer, s |
| $t_s$ | efflux time of CS solution measured by the Ubbelohde viscometer, s |
| $T$ | temperature, °C |
| $v$ | velocity of fluid, m/s |
| $V$ | volume of fluid, $m^3$ |
| $We$ | Weber number |
| $\alpha$ | geometrical parameter, 1/m |
| $\gamma$ | dimensionless parameter |
| $\rho$ | density, $kg/m^3$ |
| $\eta$ | intrinsic viscosity reduction rate, % |
| $[\eta]$ | intrinsic viscosity, L/g |
| $[\eta]_0$ | intrinsic viscosity of the initial CS solution, L/g |
| $[\eta]_1$ | intrinsic viscosity of the solution after CS degradation, L/g |
| $\eta_r$ | relative viscosity |
| $\eta_{sp}$ | specific viscosity |
| $\mu$ | viscosity, Pa·s |
| $\sigma$ | interfacial tension, N/m |
| **Subscripts** | |
| 0 | before cavitation |
| 1 | after cavitation |

## References


1. Panda, D.; Saharan, V.K.; Manickam, S. Controlled hydrodynamic cavitation: A review of recent advances and perspectives for greener processing. *Processes* **2020**, *8*, 220. [CrossRef]
2. Asaithambi, N.; Singha, P.; Dwivedi, M.; Singh, S.K. Hydrodynamic cavitation and its application in food and beverage industry: A review. *J. Food Process Eng.* **2019**, *42*, e13144. [CrossRef]
3. Wang, B.W.; Su, H.J.; Zhang, B. Hydrodynamic cavitation as a promising route for wastewater treatment-A review. *Chem. Eng. J.* **2021**, *412*, 128685. [CrossRef]
4. Bargole, S.; George, S.; Saharan, V.K. Improved rate of transesterification reaction in biodiesel synthesis using hydrodynamic cavitating devices of high throat perimeter to flow area ratios. *Chem. Eng. Process. Process Intensif.* **2019**, *139*, 1–13. [CrossRef]
5. Carpenter, J.; George, S.; Saharan, V.K. Low pressure hydrodynamic cavitating device for producing highly stable oil in water emulsion: Effect of geometry and cavitation number. *Chem. Eng. Process. Process Intensif.* **2017**, *116*, 97–104. [CrossRef]
6. Cao, Y.; Liu, X.W.; Ren, X.E.; Huang, Y.C. Removal of Fe3+ from ammonium dihydrogen phosphate solution in an impact-jet hydraulic cavitation extractor. *Arab. J. Chem.* **2022**, *15*, 103637. [CrossRef]
7. Benito, Y.; Arrojo, S.; Hauke, G.; Vidal, P. Hydrodynamic cavitation as a low-cost AOP for wastewater treatment: Preliminary results and a new design approach. *WIT Trans. Ecol. Environ.* **2005**, *80*, 495–503.
8. Panda, D.; Manickam, S. Sonochemical degradation of endocrine-disrupting organochlorine pesticide Dicofol: Investigations on the transformation pathways of dechlorination and the influencing operating parameters. *Chemosphere* **2018**, *204*, 101–108.
9. Carpenter, J.; Badve, M.; Rajoriya, S.; George, S.; Saharan, V.K.; Pandit, A.B. Hydrodynamic cavitation: An emerging technology for the intensification of various chemical and physical processes in a chemical process industry. *Rev. Chem. Eng.* **2017**, *33*, 433–468. [CrossRef]
10. Pandit, A.; Indurkar, A.; Deshpande, C.; Jain, R.; Dandekar, P. A systematic review of physical techniques for chitosan degradation. *Carbohyd. Polym. Technol. Appl.* **2021**, *2*, 100033. [CrossRef]
11. Tsao, C.T.; Chang, C.H.; Lin, Y.Y.; Wu, M.F.; Han, J.L.; Hsieh, K.H. Kinetic study of acid depolymerization of chitosan and effects of low molecular weight chitosan on erythrocyte rouleaux formation. *Carbohyd. Res.* **2011**, *346*, 94–102. [CrossRef]
12. Shi, Z.H.; Mahdavian, Y.; Mahdavian, Y.; Mahdigholizad, S.; Irani, P.; Karimian, M.; Abbasi, N.; Ghaneialvar, H.; Zangeneh, A.; Zangeneh, M.M. Cu immobilized on chitosan-modified iron oxide magnetic nanoparticles: Preparation, characterization and investigation of its anti-lung cancer effects. *Arab. J. Chem.* **2021**, *14*, 103224. [CrossRef]

13. Mei, Y.X.; Dai, X.Y.; Yang, W.; Xu, X.W.; Liang, Y.X. Antifungal activity of chitooligosaccharides against the dermatophyte Trichophyton rubrum. *Int. J. Biol. Macromol.* **2015**, *77*, 330–335. [CrossRef] [PubMed]
14. Chokradjaroen, C.; Theeramunkong, S.; Yui, H.; Saito, N.; Rujiravanit, R. Cytotoxicity against cancer cells of chitosan oligosaccharides prepared from chitosan powder degraded by electrical discharge plasma. *Carbohyd. Polym.* **2018**, *201*, 20–30. [CrossRef] [PubMed]
15. Yin, H.; Zhao, X.M.; Du, Y.G. Oligochitosan: A plant diseases vaccine—A review. *Carbohyd. Polym.* **2010**, *82*, 1–8. [CrossRef]
16. Huang, Y.C.; Wu, Y.; Huang, W.C.; Yang, F.; Ren, X.E. Degradation of chitosan by hydrodynamic cavitation. *Polym. Degrad. Stab.* **2013**, *98*, 37–43. [CrossRef]
17. Huang, Y.C.; Wang, P.F.; Yuan, Y.; Ren, X.E.; Yang, F. Synergistic degradation of chitosan by impinging stream and jet cavitation. *Ultrason. Sonochem.* **2015**, *27*, 592–601. [CrossRef]
18. Wu, Y.; Huang, Y.C.; Zhou, Y.; Ren, X.E.; Yang, F. Degradation of chitosan by swirling cavitation. *Innov. Food Sci. Emerg.* **2014**, *23*, 188–193. [CrossRef]
19. Yan, J.C.; Xu, J.L.; Ai, S.; Zhang, K.M.; Yang, F.; Huang, Y.C. Degradation of chitosan with self-resonating cavitation. *Arab. J. Chem.* **2020**, *13*, 5776–5787. [CrossRef]
20. Richard, W.J. *Handbook of Fluid Dynamics*, 2nd ed.; CRC Press: Boca Raton, FL, USA, 2016.
21. Yan, J.C.; Ai, S.; Yang, F.; Zhang, K.M.; Huang, Y.C. Study on mechanism of chitosan degradation with hydrodynamic cavitation. *Ultrason. Sonochem.* **2020**, *64*, 105046. [CrossRef]
22. Hu, Y.L.; Lu, Y.; Zhou, G.J.; Xia, X.H. A simple electrochemical method for the determination of hydroxyl free radicals without separation process. *Talanta* **2008**, *74*, 760–765. [CrossRef] [PubMed]
23. Fernández-Castro, P.; Vallejo, M.; San Román, M.F.; Ortiz, I. Insight on the fundamentals of advanced oxidation processes: Role and review of the determination methods of reactive oxygen species. *J. Chem. Technol. Biotechnol.* **2015**, *90*, 796–820. [CrossRef]
24. Shi, Q.Q.; Zhang, X.Y.; Liu, X.; Xu, L.L.; Liu, B.C.; Zhang, J.; Xu, H.; Han, Z.K.; Li, G. In-situ exfoliation and assembly of 2D/2D g-$C_3N_4$/$TiO_2$(B) hierarchical microflower: Enhanced photo-oxidation of benzyl alcohol under visible light. *Carbon* **2022**, *196*, 401–409. [CrossRef]
25. Shi, Q.Q.; Raza, A.; Xu, L.L.; Li, G. Bismuth oxyhalide quantum dots modified sodium titanate necklaces with exceptional population of oxygen vacancies and photocatalytic activity. *J. Colloid Interf. Sci.* **2022**, *625*, 750–760. [CrossRef] [PubMed]
26. Zhang, Y.F.; Wang, M.; Li, G. Recent advances in aerobic photo-oxidation over small-sized IB metal nanoparticles. *Photochem* **2022**, *2*, 528–538. [CrossRef]
27. Zupanca, M.; Petkovšeka, M.; Zevnika, J.; Kozmusa, G.; Šmidb, A.; Dular, M. Anomalies detected during hydrodynamic cavitation when using salicylic acid dosimetry to measure radical production. *Chem. Eng. J.* **2020**, *396*, 125389. [CrossRef]
28. Kumar, P.S.; Kumar, M.S.; Pandit, A.B. Experimental quantification of chemical effects of hydrodynamic cavitation. *Chem. Eng. Sci.* **2000**, *55*, 1633–1639. [CrossRef]
29. Vichare, N.P.; Gogate, P.R.; Pandit, A.B. Optimization of hydrodynamic cavitation using a model reaction. *Chem. Eng. Technol.* **2000**, *23*, 683–690. [CrossRef]
30. Zhang, X.D.; Fu, Y.; Li, Z.Y.; Zhao, Z.C. The collapse intensity of cavities and the concentration of free hydroxyl radical released in cavitation flow. *Chin. J. Chem. Eng.* **2008**, *16*, 547–551. [CrossRef]
31. Zhang, X.Y.; Zhu, X.F.; Cao, Y.; Zhang, K.M.; Huang, Y.C.; Yang, F.; Ren, X.E. Analysis of the influencing factors of the hydroxyl radical yield in a hydrodynamic cavitation bubble of a chitosan solution based on a numerical simulation. *ACS Omega* **2021**, *6*, 3736–3744. [CrossRef]
32. Wang, K.; Yu, L.X.; Yin, S.; Li, H.N.; Li, H.M. Photocatalytic degradation of methylene blue on magnetically separable FePc/$Fe_3O_4$ nanocomposite under visible irradiation. *Pure Appl. Chem.* **2009**, *81*, 2327–2335. [CrossRef]
33. Saharan, V.K.; Badve, M.P.; Pandit, A.B. Degradation of reactive red 120 dye using hydrodynamic cavitation. *Chem. Eng. J.* **2011**, *178*, 100–107. [CrossRef]
34. Mancuso, G.; Langone, M.; Andreottola, G. A critical review of the current technologies in wastewater treatment plants by using hydrodynamic cavitation process: Principles and applications. *J. Environ. Health Sci.* **2020**, *18*, 311–333. [CrossRef] [PubMed]
35. Bagal, M.V.; Gogate, P.R. Wastewater treatment using hybrid treatment schemes based on cavitation and Fenton chemistry: A review. *Ultrason. Sonochem.* **2014**, *21*, 1–14. [CrossRef] [PubMed]
36. Nikolić, I.; Jovanović, J.; Koturević, B.; Adnadjević, B. Transesterifcation of sunfower oil in the presence of the cosolvent assisted by hydrodynamic cavitation. *BioEnerg. Res.* **2022**, *15*, 1568–1578. [CrossRef]
37. Amin, L.P.; Gogate, P.R.; Burgess, A.E.; Bremner, D.H. Optimization of a hydrodynamic cavitation reactor using salicylic acid dosimetry. *Chem. Eng. J.* **2010**, *156*, 165–169. [CrossRef]
38. Randhavane, S.B.; Khambete, A.K. Harnessing hydroxyl radicals generated by hydrodynamic cavitation reactor in simultaneous removal of chlorpyrifos pesticide and COD from aqueous solution. *Desalin. Water Treat.* **2017**, *82*, 346–354. [CrossRef]
39. Randhavane, S.B.; Khambete, A.K. Hydrodynamic cavitation: An approach to degrade chlorpyrifos pesticide from real effluent. *KSCE J. Civ. Eng.* **2018**, *22*, 2219–2225. [CrossRef]
40. Zhang, X.D.; Yang, H.Z.; Li, Z.Y. Relationship between strength of hydrodynamic cavitation and amount of induced hydroxyl radical. *J. Chem. Ind. Eng.* **2007**, *58*, 27–32. (In Chinese)
41. Gogate, P.R.; Pandit, A.B. Engineering design methods for cavitational reactors. II. Hydrodynamic cavitation. *AIChE J.* **2000**, *46*, 1641–1649. [CrossRef]

42. Tao, Y.Q.; Cai, J.; Huai, X.L.; Liu, B. Global average hydroxyl radical yield throughout entire lifetime of cavitation bubbles. *Chem. Eng. Technol.* **2018**, *41*, 1035–1042. [CrossRef]
43. Jyoti, K.K.; Pandit, A.B. Water disinfection by acoustic and hydrodynamic cavitation. *Biochem. Eng. J.* **2001**, *7*, 201–212. [CrossRef]
44. Chakinala, A.G.; Gogate, P.R.; Burgess, A.E.; Bremner, D.H. Treatment of industrial wastewater effluents using hydrodynamic cavitation and the advanced Fenton process. *Ultrason. Sonochem.* **2008**, *15*, 49–54. [CrossRef] [PubMed]
45. Tao, Y.Q.; Cai, J.; Huai, X.L.; Liu, B.; Guo, Z.X. Application of hydrodynamic cavitation to wastewater treatment. *Chem. Eng. Technol.* **2016**, *39*, 1363–1376. [CrossRef]
46. Franc, J.P.; Michel, J.M. *Fundamentals of Cavitation*; Kluwer Academic Publishers: Dordrecht, The Netherlands, 2004.
47. Jomni, F.; Aitken, F.; Denat, A. Dynamics of microscopic bubbles generated by a corona discharge in insulating liquids: Influence of pressure. *J. Electrostat.* **1999**, *47*, 49–59. [CrossRef]
48. Li, G.; Ye, S.C.; Zhang, Z.G.; Ma, Y.L. Research and analysis of mass transfer model for liquid-liquid phase dispersion extraction. *J. Chem. Eng. Chin. U.* **2015**, *29*, 1325–1332. (In Chinese)
49. Cao, Y.; Li, J.; Jin, Y.; Luo, J.H.; Wang, Y.B. Liquid–liquid two-phase mass transfer characteristics in a rotating helical microchannel. *Chin. J. Chem. Eng.* **2019**, *27*, 2937–2947. [CrossRef]
50. Su, Y.H.; Chen, G.W.; Zhao, Y.C.; Yuan, Q. Intensification of liquid–liquid two-phase mass transfer by gas agitation in a microchannel. *AIChE J.* **2009**, *55*, 1948–1958. [CrossRef]
51. Liu, J.; Pu, H.M.; Zhang, X.; Xiao, L.X.; Kan, J.; Jin, C.H. Effects of ascorbate and hydroxyl radical degradations on the structural, physicochemical, antioxidant and film forming properties of chitosan. *Int. J. Biol. Macromol.* **2018**, *114*, 1086–1093. [CrossRef]
52. Kang, B.; Dai, Y.D.; Zhang, H.Q.; Chen, D. Synergetic degradation of chitosan with gamma radiation and hydrogen peroxide. *Polym. Degrad. Stabil.* **2007**, *92*, 359–362. [CrossRef]